Oxidation of Au on vicinal W(110): Role of step edges and facets

A. Varykhalov,[1,2] O. Rader,[1] V. K. Adamchuk,[2] W. Gudat,[1,3] B. E. Koel,[4] and A. M. Shikin[2]
[1]*BESSY, Albert-Einstein-Str. 15, D-12489 Berlin, Germany*
[2]*Institute of Physics, St.-Petersburg State University, St.-Petersburg 198504, Russia*
[3]*Institut für Physik, Universität Potsdam, D-14415 Potsdam, Germany*
[4]*Department of Chemistry, Lehigh University, Bethlehem, Pennsylvania 18015, USA*
(Received 11 September 2006; revised manuscript received 25 January 2007; published 11 May 2007)

The electronic and chemical properties of Au on stepped surface oxides are of great fundamental and practical interest. Vicinal W(110) substrates have been used as templates for deposition and oxidation of submonolayer amounts of Au. Crystal surfaces of flat W(110), W(145) with the densest step edges, and W(331) and W(551) with open step edges were employed as model systems. By photoemission from the 4*f* core levels of Au and W, the most dramatic changes to the ionic state of the Au, resulting in complete oxidation, were observed on preoxidized W(331) and W(551) after annealing at 900 K. By scanning tunneling microscopy, it was found that chemisorption of oxygen causes nanofaceting of the vicinal W(110) surfaces. The impact of the facets on the surface chemistry revealed by the experiment is discussed. The dimensions and periodicity of the facets were found to be a principal factor in Au oxidation.

DOI: 10.1103/PhysRevB.75.205417 PACS number(s): 68.43.Hn, 79.60.Jv, 68.37.Ef, 82.65.+r

I. INTRODUCTION

Nanometer-scaled structures of the noble metals Au and Ag supported on various oxide surfaces are the subject of intensive research since it was found that they exhibit enhanced catalytic activity, particularly for the oxidation of carbon monoxide.[1–6] Several theories and models have attempted to relate the catalytic properties to the atomic and electronic structure of these nanoclusters.[7] Although the properties and reactivity of metallic nanoclusters have been extensively studied experimentally, an understanding at an atomic level is still missing.

One explanation for the observed catalytic activity, for example, is related to quantum-size effects in the electronic structure of nanoclusters. If the clusters are small enough, the electrons of outer shells can form standing waves and discrete energy eigenvalues dominate the valence band. At particular cluster sizes, these energies may be particularly efficient for catalytic reactions. For instance, Valden *et al.*[6] have shown that Au nanoclusters with widths between 3 and 3.5 nm and a thickness of 2 monatomic layers (ML) supported on TiO_2 exhibit maximal catalytic activity in low-temperature CO oxidation. It is notable that at such dimensions they possess the electronic structure of a semiconductor with a band gap of 0.2–0.6 eV.[6,8]

Another explanation for the increased catalytic activity of Au nanoclusters relates to support phenomena, i.e., the influence of the substrate on the cluster properties. This determines the extent of the charge transfer responsible for the achievement of various oxidation states of Au.[2,3,9–12] Fu *et al.* assume that Au clusters in an *anionic* state on nanocrystalline ceria serve as the active centers for the water-gas shift catalytic reaction.[11] On the other hand, it was demonstrated[10,13] that Au nanoclusters supported on a MgO substrate possess a *cationic* Au^+ state which appears to be a key factor for CO oxidation.[10]

Yet another view focuses on the role that the substrate plays in defining the geometry of the Au nanostructures. Generally speaking, the substrate determines the length and shape of the nanocluster perimeter,[6,14,15] accessibility of the topmost atomic layer of Au (which has been established as the active reaction zone in bilayer structures[6,7]), kinetics of adsorption and bonding of reactants, and reaction activation energies.[16,17] Considering the role of the nanocluster perimeter for the realization of a catalytic reaction[18] and considering such a perimeter as a curved one-dimensional atomic defect, one should assume that an increased number of defects at the surface might enhance chemical processes.[19,20] This idea is promoted by recent reports of unprecedentedly high catalytic activity with a turnover frequency as large as $4\ s^{-1}$ which was observed for the (1×3) reconstructed Au bilayer on TiO_x in CO oxidation.[7,16] Finally, the clusters could just be passive spectators which do not participate in the chemical reactions themselves; in such a case, the reaction centers are cationic $Au^{\delta+}$ accomodated in the substrate lattice as point defects at the cluster sites.[12]

In our experiments, we have achieved a cationic oxidation state of Au atoms on a defect-rich substrate. As supporting templates we used vicinal W(110) surfaces. Vicinals are crystal faces with high Miller indices that are prepared by cutting the single crystal at a small angle relative to a low-Miller-index surface. Our W surfaces possess nanometer-scaled one-dimensional steps and terraces with constant width and high regularity over macroscopic distances, which allows the observation of superlattice effects in the electronic structure by photoemission.[21] In that sense, by "defect rich" we mean regular surfaces with a high number of periodic steps as a representation of one-dimensional atomic defects.

The vicinal W(110) surfaces were precovered by oxygen. This requires particular experimental care because it can be expected that chemisorption causes surface reconstruction leading to formation of large-scale facets with a low density of defects (see, e.g., Refs. 22 and 23 and references therein). However, on some particular W(110) vicinals, oxidation will only induce a lateral rearrangement of W atoms [as we demonstrate by scanning tunneling microscopy (STM) further

below], thus preserving the initially high density of step edges. On such particular templates we achieved complete oxidation of adsorbed Au by predeposited oxygen. We explain this effect as oxidation of Au via reduction of W atoms of the supporting substrate.

In the following, we will prove that the presence of monatomic steps and terraces is the key condition for the observed phenomena and establish the role of atomically scaled surface defects as chemical reaction centers.

II. EXPERIMENT

The experimental characterization of the chemical state of adsorbed Au and the supporting W substrates was done by photoelectron spectroscopy.[24] Energy shifts of core-level peaks observed in photoemission spectra provide valuable information about the chemical environment of the probed element and the charge transfer between constituents of a compound. The intensity of shifted components in the photoelectron spectra of Au 4*f* and W 4*f* indicates how complete the oxidation is. The geometry of the oxidized W substrates and the character and the density of steps, terraces, and facets were investigated by STM.

For our experiments we have chosen vicinal W(110) substrates with different step geometries. The atomic structure of W(145), W(331), and W(551) is illustrated in Figs. 1(b)–1(d), respectively. The step width on W(145) is 11.6 Å, while for W(331) this value is 9.5 Å and for W(551) 15.8 Å. W(331) and W(551) are structurally identical and only differ in the step width. We did not find any qualitative difference in the behavior (neither atomic nor electronic) of the these two crystals upon adsorption of oxygen, deposition of Au, and heating. The results obtained for both W(331) and W(551) reveal the same physics: thus we will display the data where the effects are more pronounced.

Due to the miscut direction, the steps on W(145) and W(331) [W(551)] surfaces are oriented differently relative to the W lattice. In the case of W(145), they are parallel to $[1\bar{1}\bar{1}]$ which gives rise to densely packed linear step edges. For W(331) and W(551) the edges are running along $[1\bar{1}0]$ so that they are open and rather possess an atomic "zigzag" profile. The edges are marked in Fig. 1 by thick solid lines. Since all three substrates possess the (110) face [Fig. 1(a)] as base plane of the terraces, all of the experiments were repeated with a flat W(110) crystal in order to extract the influence of the steps.

The sample preparation was done *in situ* as described in the following. Firstly, the crystals were carefully cleaned. The *in vacuo* cleaning procedure for vicinal W(110) (Ref. 21) does not differ principally from that for flat W surfaces.[25]

The cleanliness of the W(110), W(145), W(331), and W(551) surfaces was verified by low-energy electron diffraction (LEED) [Figs. 2(a), 2(c), and 2(e)] and by the presence of an intense surface-induced component in the photoelectron spectra of the W 4*f* core level [Figs. 4(a)–4(c), spectra (I)]. Afterward, the samples were thermally oxidized at 1500 K for 15 min in an O_2 atmosphere of 5×10^{-8} mbar. Such a temperature regime leads to the formation of a stable

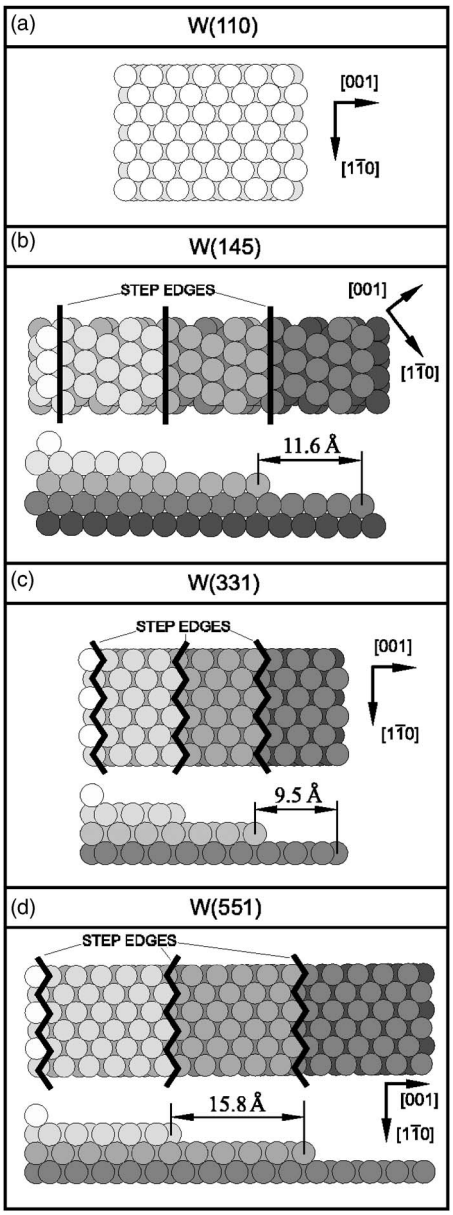

FIG. 1. Atomic structures: (a) flat W(110), (b) stepped W(145), (c) stepped W(331), and (d) stepped W(551). Different atomic layers are distinguished by a grayscale.

W surface oxide. When the oxidation was finished, the samples were flashed to 1300–1400 K in ultrahigh vacuum in order to remove nonchemically adsorbed oxygen from the surface. Afterward, the substrates were characterized by LEED again. Some results are shown in Figs. 2(b), 2(d), and 2(f). As oxygen-covered flat W(110) [Fig. 2(b)] reveals the expected $p(2\times1)$ superstructure,[26,27] which corresponds to 0.5 ML of O, but the oxidized W(145) [Fig. 2(d)] and W(331) [W(551)] [Fig. 2(f)] show more complex behavior, with the principal spots of the (110)-pattern interconnected by lines running along the high-symmetry directions of the W lattice and hosting a number of additional spots. This indicates a significant modification of the substrate geometry by the formation of facets.

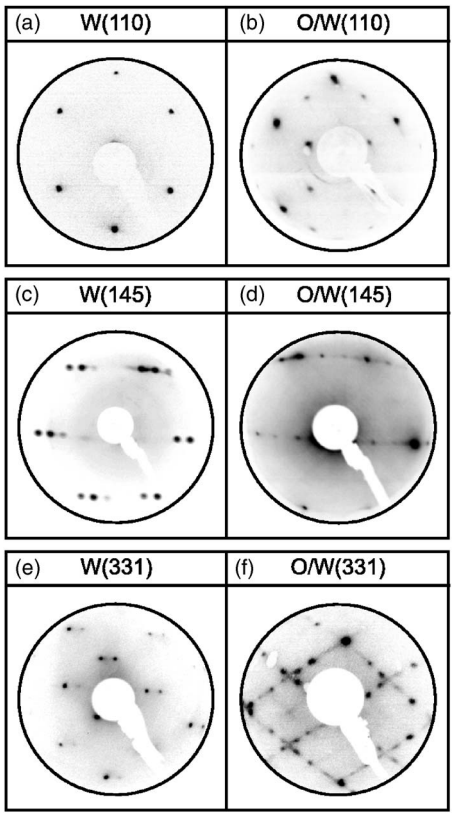

FIG. 2. LEED patterns obtained from (a) clean W(110), (b) oxidized W(110) with a $p(2\times1)$ superstructure of oxygen, (c) clean W(145), (d) oxidized W(145), (e) clean W(331), and (f) oxidized W(331). The clean stepped substrates [(c) and (e)] demonstrate in the LEED pattern a perfectly resolved superlattice of steps. The amount of oxygen on the oxidized surfaces [(b), (d), and (f)] corresponds to 0.5 ML.

The subsequent deposition of a submonolayer amount of Au onto the oxidized flat and stepped samples was done from a drop melted on a resistively heated W filament. The amount of deposited Au was carefully controlled by a quartz microbalance and by photoemission measurements. Afterward, the samples were successively annealed up to 900 K until changes appeared in the electronic structure. At each stage of the sample preparation the chemical states of Au and W atoms at the surface were probed by photoemission of 4*f* core levels. Photoelectron spectroscopy experiments were performed using a VG ESCAlab electron spectrometer at a total-energy resolution of 80 meV. Russian-German PGM (Ref. 28) and UE56/1 PGM (Ref. 29) beamlines at BESSY were employed as tunable sources of synchrotron radiation.

STM measurements were done in a separate chamber. LEED patterns were used as a reference for reproducing the oxidized W substrates. We used electrochemically etched W tips, which were able to supply high lateral resolution after extensive *in situ* treatment.[30] The base pressure during the experiments was about 1×10^{-10} mbar.

III. RESULTS AND DISCUSSION

A. Photoemission from Au 4*f*

Before considering the question of the substrate geometry further, we will give an overview of the results of the photoemission investigation. Figure 3 presents the photoemission spectra from the $4f_{7/2}$ core level of Au deposited on preoxidized W(110) [Fig. 3(b)], W(145) [Fig. 3(c)], and W(331) [Fig. 3(d)]. All of the spectra presented are decomposed into their spectral components.[31] The spectra shown have been recorded at different stages of the sample preparation: those plotted as open circles (mark I) correspond to 0.5 ML of Au "as deposited" onto the oxygen-covered W substrates at room temperature, while the spectra plotted with filled circles (mark II) were measured after a short annealing of the samples at 900 K. The upper panel [Fig. 3(a)] contains the photoemission spectrum of a 2-ML-thick Au film grown on a clean, nonoxidized W(145). Since one can assume that for the concentrations of Au given above, the height of Au clusters on W vicinals will not exceed two to three atomic layers[6] and the Au 4*f* core level spectrum of 2-ML-thick Au grown in the layer-by-layer mode[32] on clean stepped W can be used as a reference. The reference spectrum shown in Fig. 3(a) is dominated by the bulk peak at 84.0 eV binding energy. The components located at higher binding energies of 84.2 and 84.8 eV are assigned to reduced coordination numbers of Au atoms in the topmost atomic layer and at the step edges.

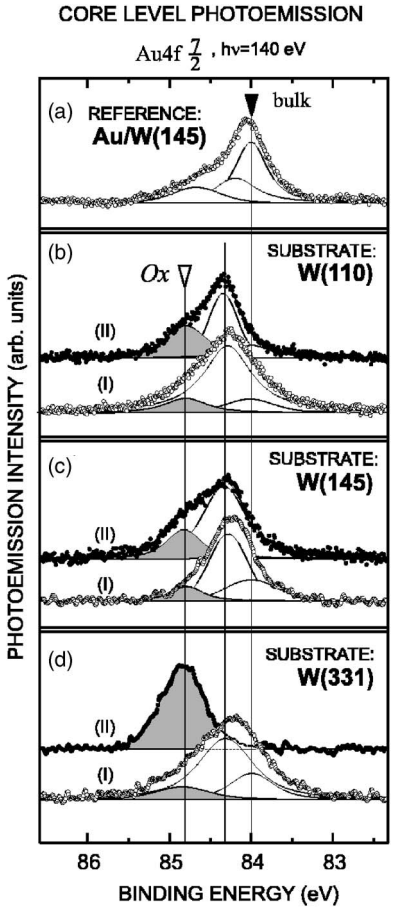

FIG. 3. Photoemission from Au $4f_{7/2}$. (a) Reference spectrum of 2-ML-thick Au on clean W(145). Panels (b)–(d) display spectra from 0.5 ML Au on (b) preoxidized flat W(110), (c) oxidized W(145), and (d) oxidized W(331). Spectra plotted with open circles (mark I) were measured from "as deposited" Au. Those plotted with filled circles (mark II) were recorded after annealing at 900 K.

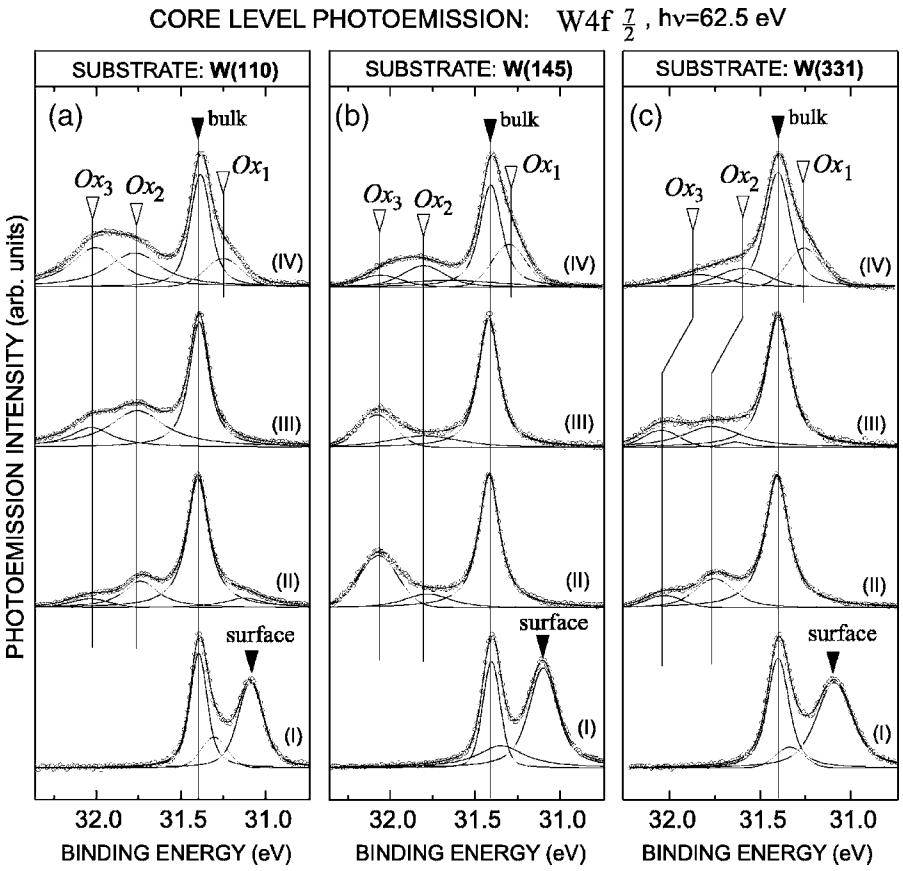

FIG. 4. Characterization of the chemical state of W by photoemission from the W $4f_{7/2}$ core level. Panels (a), (b), and (c) present spectra from W(110), W(145), and W(331), respectively. Roman numerals near each spectrum denote different stages of the sample preparation: (I) clean surface, (II) oxidized sample with $p(2\times1)$ superstructure of oxygen, (III) oxidized substrate with a submonolayer amount of Au "as deposited" at room temperature, and (IV) sample with Au oxidized by annealing at 900 K.

As can be seen from Fig. 3 (spectra I), the $4f$ spectral shape (and correspondingly the chemical state) of Au "as deposited" is nearly the same for all three oxidized samples. It is notable that for submonolayer amounts of Au, the main spectral component appears at 84.3 eV and bulklike emission at 84.0 eV is very weak. This is evidence of reduced coordination. After annealing at 900 K (spectra II), significant changes appear in the spectrum of Au on oxidized W(331) [Fig. 3(d)]. The intensity of the peak located at the highest binding energy (84.8 eV) [labeled in Fig. 3 as *Ox* and shaded in gray] increases drastically. At the same time, the other two spectral components (bulk and lower coordinated) vanish almost completely. Although some increase of the *Ox* intensity is also detected for W(145) and W(110), the effect is pronounced only for W(331) and W(551). The binding energy of the *Ox* component of Au $4f_{7/2}$ (84.8 eV) is less than that observed for Au_2O_3 (85.9 eV).[33] We note, however, that the two Au $4f$ components are 0.5 eV apart which corresponds to the energy difference between Au_2O and Au_2O_3.[34]

B. Photoemission from W 4*f*

In our experiments, we have also carefully investigated the chemical state of the W substrate at every stage of sample preparation. The changes in the ionic state of Au are accompanied by a notable charge redistribution between W and O. We observed that the increase in the degree of Au oxidation induced a corresponding decrease in the oxidation of W. This effect was detected in W $4f_{7/2}$ core-level spectra which were measured at $h\nu$=62.5 eV. The three panels in Fig. 4 represent the spectra obtained for (a) W(110), (b) W(145), and (c) W(331) substrates. Spectra tracing the various sample treatments are marked by roman numerals: (I) clean W surfaces, (II) oxidized W samples with a $p(2\times1)$ superstructure of oxygen, (III) oxidized substrates with a submonolayer amount of Au "as deposited" at room temperature, and (IV) samples with Au oxidized by annealing at 900 K.

Oxidation on all three W crystals caused the surface-induced peak [Fig. 4(I)] of the W $4f$ core level to vanish.[27,35] At the same time, two new components appear: Ox_2 at ~31.7 eV and Ox_3 at ~32.1 eV binding energy. They originate from W atoms that have two-fold and three-fold coordinations to the adsorbed oxygen, respectively.[27] It is also notable that at the beginning the oxidation state of all three W surfaces is different, which is reflected by different ratios between the intensities of the Ox_2 and Ox_3 peaks. Especially pronounced is the case of W(145) [Fig. 4(b), spectrum (II)], where Ox_2 is almost absent.

The deposition of Au onto the oxidized samples at room temperature does not significantly modify the chemical state of W substrates as one sees from the behavior of the Ox_2 and Ox_3 intensities, which are nearly preserved [Fig. 4, spectra (III)]. This agrees with the Au $4f$ spectra that appear to be almost the same on all three W substrates for as deposited Au [Fig. 3, spectra(I)]. After annealing, however, notable changes appear in the W $4f$ photoemission [Fig. 4, spectra (IV)]. While the intensities of Ox_3 and Ox_2 spectral components are preserved after annealing or even slightly increase for the flat W(110), the intensity of peak Ox_3 obviously decreases for vicinal W(110) samples. Moreover, for W(331)

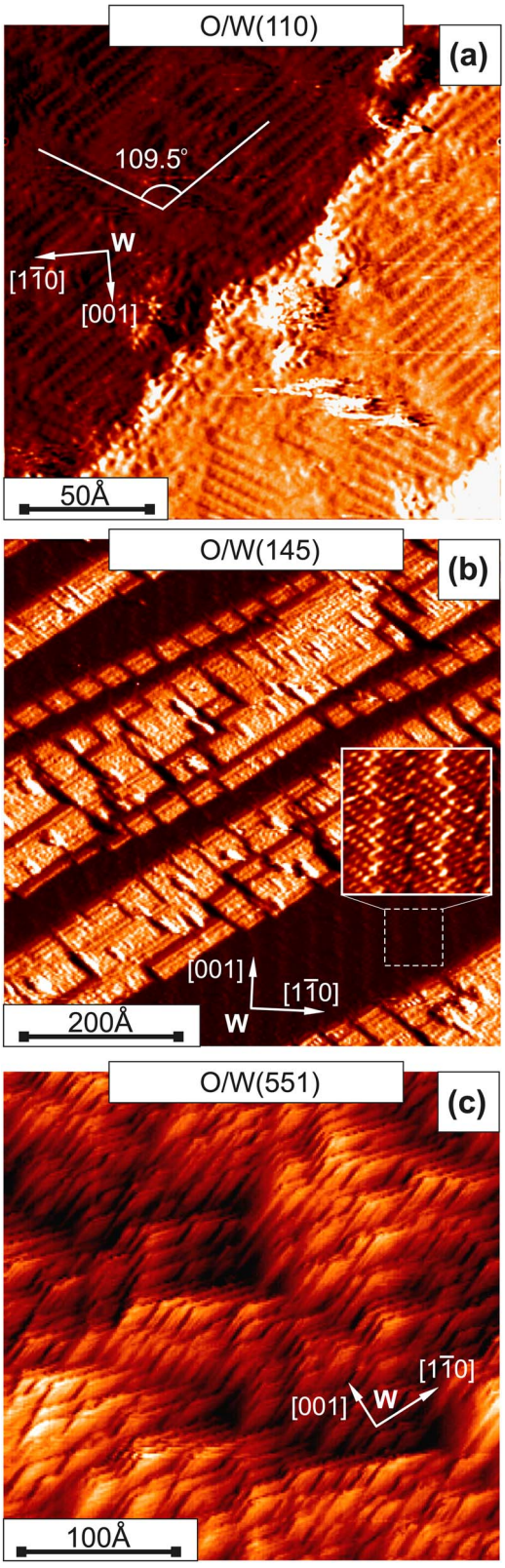

FIG. 5. (Color online) STM investigation. (a) Reference system O/W(110): $p(2\times1)$ domains rotated by 109.5° are visible. (b) O/W(145): Large-scale faceting is revealed. The base plane (110) (bright areas) is patterned by terraces of parallelogram shape (nanofacets). (c) O/W(551): The sample surface is uniformly patterned by triangular nanofacets.

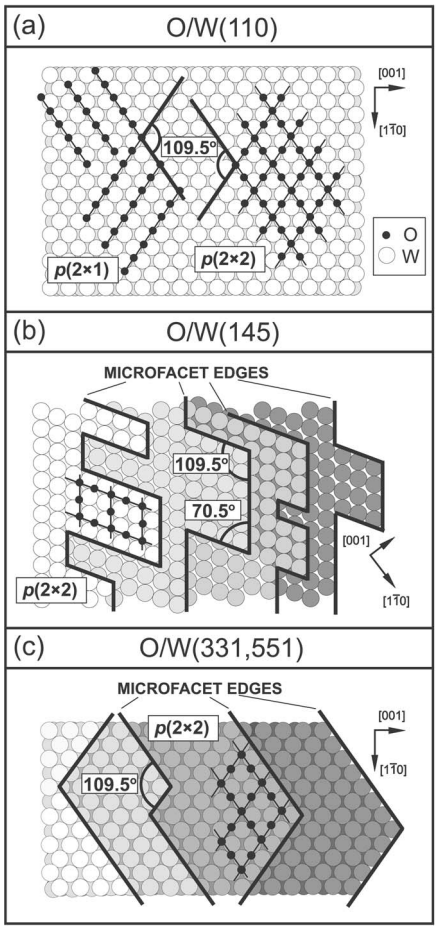

FIG. 6. (a) $p(2\times1)$ and $p(2\times2)$ superstructures of oxygen on W(110), (b) geometry of nanofacets on O/W(145), and (c) geometry of nanofacets on O/W(331) and O/W(551). Facet edges are marked by thick solid lines.

both satellite peaks undergo a notable shift by 0.25 eV toward lower binding energy meaning weakening of O-W chemical bonding as a result of a change in coordination of O atoms relative to the W substrate. An apparent relocation of oxygen away from the substrate agrees with Au-O chemical bonding, the formation of which is revealed by Au $4f$ core-level spectra (Fig. 3). Weakening of the chemical interaction between O and W substrates after annealing is further supported by the appearance of the Ox_1 spectral component at about 31.25 eV [spectra (IV) in Figs. 4(a)–4(c)]. The peak Ox_1 originates from W atoms in which the oxidation state is lowest due to the lowest possible one-fold coordination to oxygen.[27,35] To sum up about the system Au/O/W(331), we observe switching of the oxidation (cationic) state from W to Au.

The key question is why this effect is strongly pronounced when the oxidized W(331) [W(551)] is used as substrate but is almost not observed for W(145), just as with flat W(110). It is tempting to invoke the different geometries of the step edges at these surfaces (Fig. 1). However, according to LEED (Fig. 2), vicinals of W(110) undergo certain modifications upon oxygen adsorption that do not preserve their initial structures as shown in Fig. 1. To understand the exact

geometry, a real-space characterization of the surface geometry is needed.

C. Characterization by STM

Figure 5 shows STM images from all three W samples that were oxidized according to the procedure described in the experimental section. In order to emphasize both the large corrugations in the surface topography and the fine atomic structures, the images are presented after a correction which combines the topography signal with its derivative and subtracts the overall slope.

Figure 5(a) displays the oxidized flat W(110) with 0.5 ML of oxygen arranged at the surface in the well-known $p(2\times1)$ superstructure.[26] One clearly sees two types of atomically resolved domains of oxygen rotated by 109.5°. Below, we put forward a model which illustrates how the geometry of the oxygen superstructure takes control over the reconstruction of stepped oxidized W surfaces. For the sake of clarity, we use in our model a symmetric $p(2\times2)$ superstructure (0.75 ML O) which is locally identical to $p(2\times1)$. Atomic structures of $p(2\times1)$ and $p(2\times2)$ reconstructions are schematically shown in Fig. 6(a).

The STM image in Fig. 5(b) was obtained from the oxidized W(145) surface, the LEED pattern of which is displayed in Fig. 1(d). Apparently, the periodic array of steps was no longer maintained. Instead, strong faceting can be seen. Facets are one-dimensional, take on a mean periodicity of 200 Å, and run along $[1\bar{1}\bar{1}]$, i.e., along the direction of the original steps. The angle between the sides of the facets measured in the mirror plane along z is nearly 167°. On one side of each facet (bright areas) a multitude of parallelogram-shaped smaller terraces (nanofacets) is visible, while the other side (dark areas) is flat and hosts a certain large-scale superstructure of oxygen with unit-cell dimensions of $(55\pm1)\times(11\pm1)$ Å^2. An atomically resolved STM image from this dark area is given as inset to Fig. 5(b). The nanofacet-rich areas which are imaged brightly in Fig. 5(b) correspond to the former base plane of steps (110); this is concluded since oxygen rows of $p(2\times1)$ superstructure are visible in these areas. The STM measurements show that the structure of the small parallelogram-shaped terraces is caused by the geometry of the oxygen-induced reconstruction [Fig. 6(a)]. The atomic structure of the nanofacets is sketched in Fig. 6(b): as the surface oxide is formed, a substantial transfer of substrate material occurs so that W atoms are redistributed following exactly the geometry of the oxygen matrix. The nanofacets possess characteristic angles of 109.5° and 70.5° and the measured corrugation is ~3 Å, which corresponds to the single-step height.

The properties of the other plane of the facet [dark regions in Fig. 5(b)] which hosts a novel oxygen reconstruction must be the subject of a more specialized future publication, especially for a correct interpretation of the photoemission results for W(145). It may be that the anomalously intense spectral component Ox_3 of W $4f$ [Fig. 4(b)] does not originate from the oxygen-covered (110) face but is induced by this new superstructure.

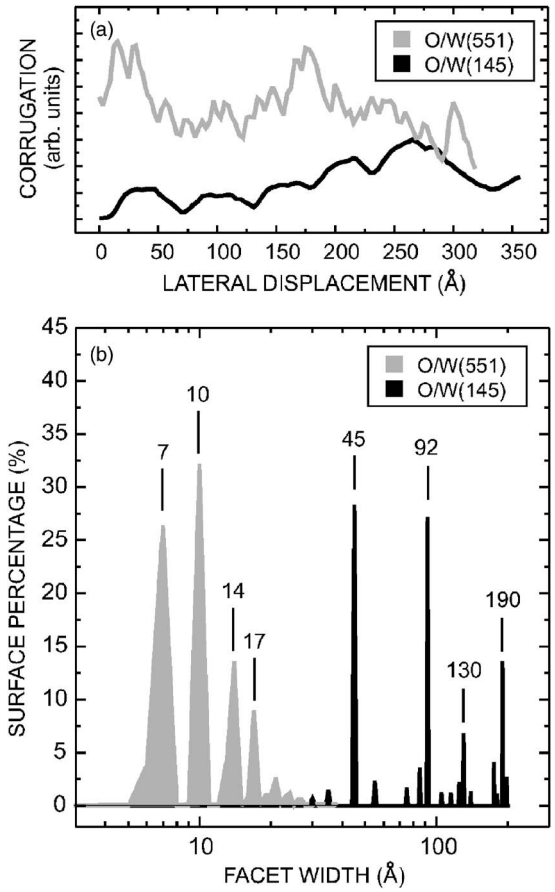

FIG. 7. Geometric characterization of the oxygen-induced nanofacets. (a) Characteristic topographic profiles across the nanofacets [from Figs. 5(b) and 5(c)]. (b) Statistical analysis of the nanofacet widths in the STM data; the gray color denotes O/W(551) and the black color corresponds to O/W(145).

We would like to proceed with the investigation of the oxygen-induced surface reconstruction on W(331) and W(551). Since no qualitative difference was found either in photoemission or STM experiments between W(551) and W(331), we limit ourselves to showing STM data for W(551). Figure 5(c) displays an image from oxidized W(551). It reveals an adsorbate-induced substrate modification in some sense similar to the case of W(145), however, with large-scale facets without different crystallographic planes. Oxidized W(551) possesses a complex self-organized surface with nanofacets derived from the (110) base plane of the initial terraces across the whole sample area. These nanofacets are of triangular shape with monatomic steps under angles of 109.5° with a measured corrugation of ~2 Å. The atomic structure of the oxidized W(331) [W(551)] is illustrated in Fig. 6(c). It is evident that exactly as in the case of nanofacet formation on W(145) the geometry of the nanofacets is due to the rearrangements of W atoms as a result of oxygen adsorption into $p(2\times2)$ and $p(2\times1)$ superstructures.

D. The role of the step edges

A more elaborate analysis of the STM data reveals in detail how the geometry of the oxidized substrates influences

the partial oxidation of Au. Recalling the photoemission spectra of Au and W core levels [Figs. 3 and 4], the most pronounced energy shifts related to the oxidation of Au and concomittant reduction of W were observed in the case of W(331) [W(551)], while for W(145) the situation was almost the same as for the flat W(110) surface. The key factor which determines the changing chemical bonding between W and Au is the enhanced coordination of Au atoms to the oxidized substrates. This can obviously be realized at the edges of steps and facets. Referring to the structural models of O/W(145) [Fig. 6(b)] and O/W(331) [Fig. 6(c)], one might speculate that the difference in chemical reactivity arises from the difference in the angles between the nanofacet edges (70.5° and 109.5°). These angles determine the atomic coordination of Au atoms nested at the kinks. However, the overall area occupied by the kinks of this type is negligible.

Other locations where adsorbed Au atoms can gain enhanced coordination to the substrate are step edges. We have statistically investigated our STM data for periodicities of the oxygen-induced nanofacets on W(145) and W(551). Figure 7(a) displays typical topography profiles of oxidized W(145) and W(551) extracted from Figs. 5(b) and 5(c). The line sections were taken along the direction perpendicular to the original steps of the clean vicinal W(110) substrates [along [001] for W(551) and perpendicular to $[1\bar{1}\bar{1}]$ for W(145)]. Comparing the profile of oxidized W(145) (black line) with that of oxidized W(551) (gray line) reveals that the average periodicity of nanofacets on W(551) is significantly smaller [on W(331) it is even less due to initially narrower terraces]. The statistics of nanofacet dimensions accumulated for O/W(551) and O/W(145) in multiple STM measurements are presented in Fig. 8(b). The facet widths of oxidized W(551) have statistical maxima at 7 and 10 Å in contrast to the case of oxidized W(145) for which the most probable widths are by an order of magnitude larger: 45 and 92 Å. The effective area occupied by edges of nanofacets on oxidized W(331) is about six to eight times larger than on oxidized W(145). This correlates well with the spectroscopic results (Fig. 3) which revealed a dramatic increase in the intensity of the oxidation-induced peak *Ox* for Au on oxidized W(331) [W(551)].

Summing up, we conclude that the oxidation state of Au atoms at the surface and switching of the oxidized species from W to Au exclusively takes place at the edges of steps and facets which pattern an ultrathin layer of surface oxide periodically, playing the role of one-dimensional atomic defects. This requires the Au to be dispersed at these sites which apparently occurs as a result of lateral Au diffusion after annealing the samples at 900 K.

IV. SUMMARY

In summary, we have investigated the nature and extent of oxidation of submonolayer amounts of Au deposited on the W(110) vicinal substrates W(331), W(551), and W(145) precovered by oxygen. Using photoemission of the chemically sensitive core levels Au $4f$ and W $4f$, a switching of the oxidized metallic species from the W substrate to Au adatoms was observed at the elevated temperature of 900 K. The fraction of oxidized Au was found to be strongly dependent on the atomic structure of steps on the particular substrate. With the help of STM, we have established an adsorbate-induced nanofaceting of W(110) vicinals upon chemisorption of oxygen. The observed density of facets on oxidized W(331) [W(551)] was found to be one order of magnitude higher than on oxidized W(145) and the comparative analysis performed for these two samples leads us to conclude that the Au oxidation takes place at the edges of steps (nanofacets) which pattern the substrate and act like one-dimensional atomic defects accomodated in the ultrathin surface oxide.

ACKNOWLEDGMENTS

We thank A. M. Ionov and S. N. Bozko for kindly lending us the W(145) crystal. This work was supported by DFG (RA 1041/1-1 and 436RUS113/735/0-2), common DFG-RFBR (06-02-04008) and RFBR (07–02–00809) projects, FCNTP programs of Russia (02.518.11.7029), and in the framework of "Scientific School" (9826.2006.2). B.E.K. acknowledges support by the National Science Foundation under Grant No. 0213583.

[1] R. Meyer, C. Lemire, S. K. Shaikhutdinov, and H. Freund, Gold Bull. **37**, 72 (2004).
[2] M. Haruta, Catal. Today **36**, 153 (1997).
[3] C. R. Henry, Surf. Sci. Rep. **31**, 231 (1998).
[4] A. Sanchez, S. Abbet, U. Heiz, W.-D. Schneider, H. Hakkinen, R. S. Barnett, and U. Landmann, J. Phys. Chem. A **103**, 9573 (1999).
[5] U. Heiz and W.-D. Schneider, J. Phys. D **33**, R85 (2000).
[6] M. Valden, X. Lai, and D. W. Goodman, Science **281**, 1647 (1998).
[7] M. S. Chen and D. W. Goodman, Catal. Today **111**, 22 (2006).
[8] D. W. Goodman, Catal. Lett. **99**, 1 (2005).
[9] V. Schwartz, D. R. Mullins, W. F. Yan, B. Chen, S. Dai, and S. H. Overbury, J. Phys. Chem. B **108**, 15782 (2004).
[10] J. Guzman and B. C. Gates, J. Am. Ceram. Soc. **126**, 2672 (2004).
[11] Q. Fu, H. Saltsburg and M. Flytzami-Stephanopoulos, Science **301**, 935 (2003).
[12] R. J. Davis, Science **301**, 926 (2003).
[13] J. Guzman and B. C. Gates, J. Phys. Chem. B **106**, 7659 (2002).
[14] M. Valden, S. Pak, X. Lai, and D. W. Goodman, Catal. Lett. **56**, 7 (1998).
[15] L. Guzzi, G. Peto, A. Beck, K. Frey, O. Geszti, G. Molnar, and C. Daroczi, J. Am. Ceram. Soc. **125**, 4332 (2003).
[16] M. S. Chen and D. W. Goodman, Science **306**, 252 (2004).
[17] M. Maciejewski, P. Fabriziolli, J. D. Grunwaldt, O. S. Beckert, and A. Baiker, Phys. Chem. Chem. Phys. **3**, 3846 (2001).
[18] Z. P. Liu, X. Q. Gong, J. Kohanoff, C. Sanchez, and P. Hu, Phys.

Rev. Lett. **91**, 266102 (2003).
[19] J. A. Rodriguez, G. Liu, T. Jirsak, J. Hebeck, Z. P. Chang, J. Dvorak, and A. Maiti, J. Am. Ceram. Soc. **124**, 5242 (2002).
[20] N. Lopez, J. K. Norskov, T. V. W. Janssens, A. Carlsson, A. Puig-Molina, B. S. Clausen, and J. D. Grunwaldt, J. Catal. **225**, 86 (2004).
[21] A. M. Shikin, A. Varykhalov, G. V. Prudnikova, V. K. Adamchuk, W. Gudat, and O. Rader, Phys. Rev. Lett. **93**, 146802 (2004).
[22] J. C. Tracey and J. M. Blakely, Surf. Sci. **13**, 313 (1968).
[23] A. Szczepkowicz, A. Ciszewski, R. Bryl, C. Oleksy, C.-H. Nien, Q. Wu, and T. E. Madey, Surf. Sci. **599**, 55 (2005).
[24] S. Hüfner, *Photoelectron Spectroscopy: Principles and Applications* (Springer, Berlin, 1995).
[25] R. G. Musket, W. McLean, C. A. Colmenares, D. M. Makowiecki, and W. J. Siekhaus, Appl. Surf. Sci. **10**, 143 (1982).
[26] K. E. Johnson, R. J. Wilson, and S. Chiang, Phys. Rev. Lett. **71**, 1055 (1993).
[27] D. M. Riffe and G. K. Wertheim, Surf. Sci. **399**, 248 (1998).
[28] S. I. Fedoseenko, D. V. Vyalikh, I. E. Iossifov, R. Follath, S. A. Gorovikov, R. Püttner, J. S. Schmidt, S. L. Molodtsov, V. K. Adamchuk, W. Gudat, and G. Kaindl, Nucl. Instrum. Methods Phys. Res. A **505**, 718 (2003).
[29] K. J. S. Sawhney, F. Senf, M. Scheer, F. Schäfers, J. Bahrdt, A. Gaupp, and W. Gudat, Nucl. Instrum. Methods Phys. Res. A **390**, 395 (1997).
[30] A. Varykhalov, O. Rader, and W. Gudat, Phys. Rev. B **72**, 115440 (2005).
[31] In order to decompose the Au $4f_{7/2}$ and W $4f_{7/2}$ spectra, Voigt functions have been used. Typical values for full width at half maximum (FWHM) ω_L (Lorenzian) and FWHM ω_G (Gaussian), which supplied the best fitting results, were ω_L=0.05–0.10 eV and ω_G=0.15–0.20 eV. The asymmetry parameter was neglected.
[32] A. M. Shikin, A. Varykhalov, V. K. Adamchuk, A. Ionov, S. N. Bozko, W. Gudat W, and O. Rader, J. Electron Spectrosc. Relat. Phenom. **144**, 341 (2005).
[33] C. R. Aita and N. C. Tran, J. Vac. Sci. Technol. A **9**, 1498 (1991).
[34] J. J. Pireaux, M. Liehr, P. A. Thiry, J. P. Delrue, and R. Caudano, Surf. Sci. **141**, 221 (1984).
[35] R. X. Ynzunza, R. Denecke, F. J. Palomares, J. Morais, E. D. Tober, Z. Wang, F. J. G. de Abajo, J. Liesegang, Z. Hussain, M. A. Van Hove, and C. S. Fadley, Surf. Sci. **459**, 69 (2000).